Embrittlement of a Platinum-Iridium Screen

10 January 1999

Prepared by

G. L. STECKEL and N. MARQUEZ
Mechanics and Materials Technology Center
Technology Operations

Prepared for

SPACE AND MISSILE SYSTEMS CENTER
AIR FORCE MATERIEL COMMAND
2430 E. El Segundo Boulevard
Los Angeles Air Force Base, CA 90245

19990406 080

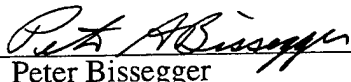Engineering and Technology Group

**THE AEROSPACE
CORPORATION**
El Segundo, California

DTIC QUALITY INSPECTED 2

This report was submitted by The Aerospace Corporation, El Segundo, CA 90245-4691, under Contract No. F04701-93-C-0094 with the Space and Missile Systems Center, 2430 E. El Segundo Blvd., Los Angeles Air Force Base, CA 90245. It was reviewed and approved for The Aerospace Corporation by P. D. Fleischauer, Principal Director, Mechanics and Materials Technology Center. P. Bissegger was the project officer for the Mission-Oriented Investigation and Experimentation (MOIE) program.

This report has been reviewed by the Public Affairs Office (PAS) and is releasable to the National Technical Information Service (NTIS). At NTIS, it will be available to the general public, including foreign nationals.

This technical report has been reviewed and is approved for publication. Publication of this report does not constitute Air Force approval of the report's findings or conclusions. It is published only for the exchange and stimulation of ideas.

Peter Bissegger
SMC/AXES

REPORT DOCUMENTATION PAGE

Public reporting burden for this collection of information is estimated to average 1 hour per response, including the time for reviewing instructions, searching existing data sources, gathering and maintaining the data needed, and completing and reviewing the collection of information. Send comments regarding this burden estimate or any other aspect of this collection of information, including suggestions for reducing this burden to Washington Headquarters Services, Directorate for Information Operations and Reports, 1215 Jefferson Davis Highway, Suite 1204, Arlington, VA 22202-4302, and to the Office of Management and Budget, Paperwork Reduction Project (0704-0188), Washington, DC 20503.

1. AGENCY USE ONLY (*Leave blank*)	2. REPORT DATE 10 January 1999	3. REPORT TYPE AND DATES COVERED

4. TITLE AND SUBTITLE

Embrittlement of a Platinum-Iridium Screen

5. FUNDING NUMBERS

F04701-93-C-0094

6. AUTHOR(S)

G. L. Steckel and N. Marquez

7. PERFORMING ORGANIZATION NAME(S) AND ADDRESS(ES)

The Aerospace Corporation
Technology Operations
El Segundo, CA 90245-4691

8. PERFORMING ORGANIZATION REPORT NUMBER

TR-99(8565)-2

9. SPONSORING/MONITORING AGENCY NAME(S) AND ADDRESS(ES)

Space and Missile Systems Center
Air Force Materiel Command
2430 E. El Segundo Boulevard
Los Angeles Air Force Base, CA 90245

10. SPONSORING/MONITORING AGENCY REPORT NUMBER

SMC-TR-99-09

11. SUPPLEMENTARY NOTES

12a. DISTRIBUTION/AVAILABILITY STATEMENT

Approved for public release; distribution unlimited

12b. DISTRIBUTION CODE

13. ABSTRACT (*Maximum 200 words*)

Following successful acceptance testing on a hydrazine Rocket Engine Module (REM), small metallic particles were discovered in a nozzle bag. It was determined that the metallic particles were segments from a Pt-15wt%-Ir screen that is used to separate coarse and fine mesh catalyst particles within the thrust chamber. One of three screens had numerous brittle, intergranular fractures at bend points of the woven wires. A failure analysis was performed by the Mechanics and Materials Technology Center (MMTC) of The Aerospace Corporation to supplement analyses performed by the spacecraft contractor and the REM manufacturer. Secondary-ion mass spectroscopy (SIMS) was used to determine the presence of any chemical contamination and revealed significant levels of gallium, indium, manganese, and copper on the wire surfaces adjacent to intergranular cracks. Tensile testing of wires extracted from the embrittled screen indicated a ductile fracture mode at 23 and 300°C (73 and 570°F), but a brittle, intergranular mode at 900°C (1650°F), indicating that the screen probably fractured during test firing of the REM. Although the cause of the screen failure was not unequivocally determined, it was concluded that contamination of the wire by indium and gallium probably caused the embrittlement. The mechanism of the failure was believed to be either liquid-metal embrittlement or the formation of low-melting-point phases at the grain boundaries.

14. SUBJECT TERMS Platinum-iridium alloys, Platinum alloys, Hydrazine motors, liquid-metal embrittlement	15. NUMBER OF PAGES 31
	16. PRICE CODE

17. SECURITY CLASSIFICATION OF REPORT UNCLASSIFIED	18. SECURITY CLASSIFICATION OF THIS PAGE UNCLASSIFIED	19. SECURITY CLASSIFICATION OF ABSTRACT UNCLASSIFIED	20. LIMITATION OF ABSTRACT

NSN 7540-01-280-5500

Acknowledgments

Contents

Figures

Tables

1. Introduction

1.1　Background

Following acceptance testing on a hydrazine Rocket Engine Module (REM), small metallic particles were discovered in a nozzle bag. The nozzle bag is used to catch any catalyst particles that escape during vibration testing, handling, transportation, etc. Analysis of the particles at the spacecraft contractor's facilities indicated that they were fragments of 0.010-in.-diam platinum-rich wire. The fragments were approximately 0.030-in. long and had brittle, intergranular fracture surfaces on both ends of the wire.

The REM is a 100-lb-force hydrazine motor built and tested by Kaiser Marquardt.[1] The motor in question is serial number (S/N) KM004. A schematic drawing of the REM is shown in Figure 1, and a blow-up of the thrust chamber and nozzle assembly is shown in Figure 2. The thrust chamber has two sets of platinum-15wt%-iridium wire screen assemblies. An end retainer/screen assembly is located at the interface between the thrust chamber and nozzle and is used to prevent catalyst particles from exiting the thrust chamber through the nozzle. This assembly has two identical Pt-Ir screens. The screens have a square weave of 0.010-in.-diam wires with 40 wires/in. Thus, the mesh openings are approximately 0.015-in.-wide squares. The two screens are placed back-to-back and oriented 45° to one another to minimize the opening size. The screens are backed-up by a curved Inconel 600 plate having approximately 0.5-in.-diam holes for gas flow. During manufacturing, dimples are formed on the screens by a hydroforming process. These dimples fit into the holes in the Inconel plate.
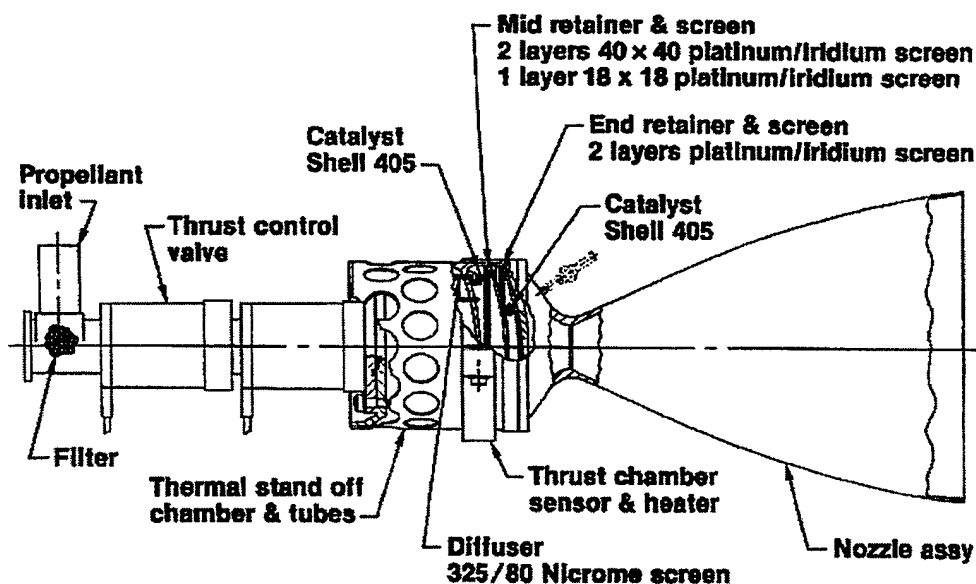
Figure 1. Spacecraft contractor drawing of rocket engine module.
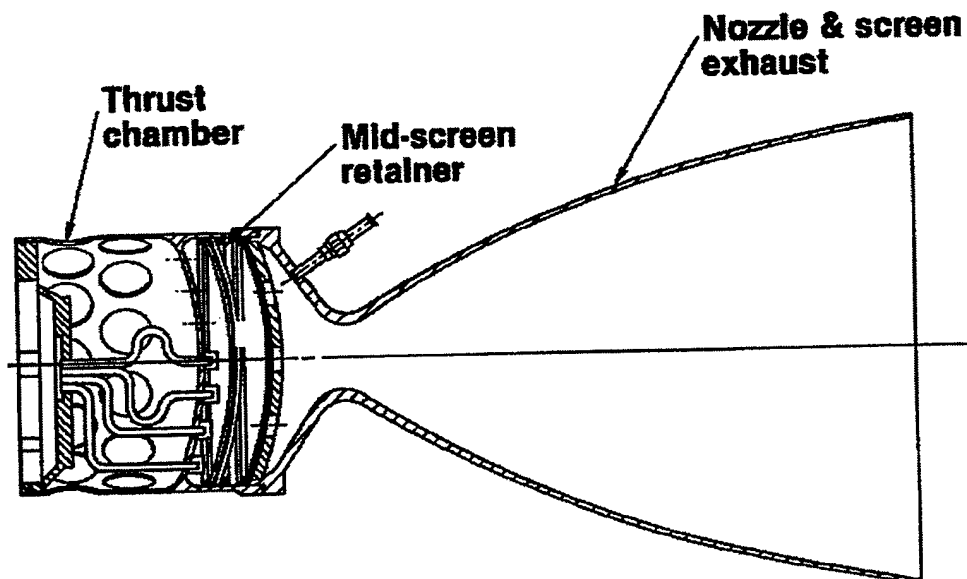
Figure 2. Spacecraft contractor drawing of thrust chamber and nozzle.

A second retainer/screen assembly is located within the catalyst bed of the thrust chamber. This assembly is referred to as the mid-retainer/screen assembly, and its function is to separate fine catalyst particles on the thrust chamber side of the retainer from coarse catalyst particles on the nozzle side. The mid-retainer/screen assembly also has two layers of the 40 x 40 wire mesh, but is stiffened and strengthened by a third layer of an 18 x 18 mesh of 0.017-in.-diam Pt-15wt%-Ir wire. This screen does not require the Inconel plate. Both screen assemblies have a concave geometry with the direction of curvature toward the nozzle. The Inconel plate and the 18 x 18 mesh screen are on the convex, nozzle side of the assemblies and, therefore, support the finer-mesh screens during motor firing.

It was anticipated that the wire fragments were coming from one or more of the 40 x 40 mesh screens. A boroscope inspection by the contractor of the end screens at the holes in the Inconel plate gave no evidence of fractures within the outer, most visible screen, but did indicate potential fractures within the inner screen. However, upon removal of the nozzle, it was discovered that neither of the two end screens were damaged. They did, however, have several wire fragments trapped within the screen openings, which probably caused the erroneous boroscope observations. Further disassembly to allow inspection of the mid-screens revealed numerous wire fractures within the first 40 x 40 mesh screen of this assembly. The second 40 x 40 mesh screen (middle screen) and the 18 x 18 mesh screen had no visible damage.

1.2 Preliminary Failure Analysis by Spacecraft Contractor

There was approximately a two-month delay between discovery of the wire fragments and the eventual disassembly of the motor discussed above. Thus, a preliminary failure analysis was performed on the wire fragments retrieved from the nozzle bag. Initially, scanning electron microscopy (SEM) utilizing energy dispersive X-rays (EDX) for chemical analyses was performed. SEM revealed the brittle intergranular nature of the fracture surfaces as shown in Figure 3. It is also apparent from

2

Figure 3 that the grain size of the Pt-Ir wire was unusually large. The ASTM grain size was approximately No. 7, which corresponds to an average grain diameter of 32 µm. It was also determined that the fractures consistently occurred at mesh bend points on the wires as shown in Figure 4. EDX indicated that the wire composition was approximately 88wt% Pt and 12wt% Ir. The only other element detected on the wire fractures or outer wire surfaces was aluminum. The presence of Al was attributed to catalyst particles that consist of Ir on an Al_2O_3 carrier. Catalyst particles can be seen on the fracture surface in Figure 3. No potentially embrittling contaminants were identified on the wire fracture surfaces.

The spacecraft contractor also performed Auger Electron Spectroscopy (AES), which indicated the presence of silicon on the fracture surfaces and on the outer wire surfaces. Elemental mapping indicated that Si was preferentially located on the tensile side of wire bends on the fracture surfaces. This was considered a potentially significant finding since it suggested that the Si may have been present prior to fracture and may have contributed to the failure. It is well documented that a low-melting-point (830°C) eutectic occurs in the Pt-Si phase diagram at approximately 4wt% Si, which causes brittle intergranular failures[2-5]. On the other hand, the presence of Si on the tensile side of the fracture surfaces may also be explained by silicon contamination of an already existing crack on the tensile side of the wire bends. In that case, the Si would be incidental to the wire fractures.
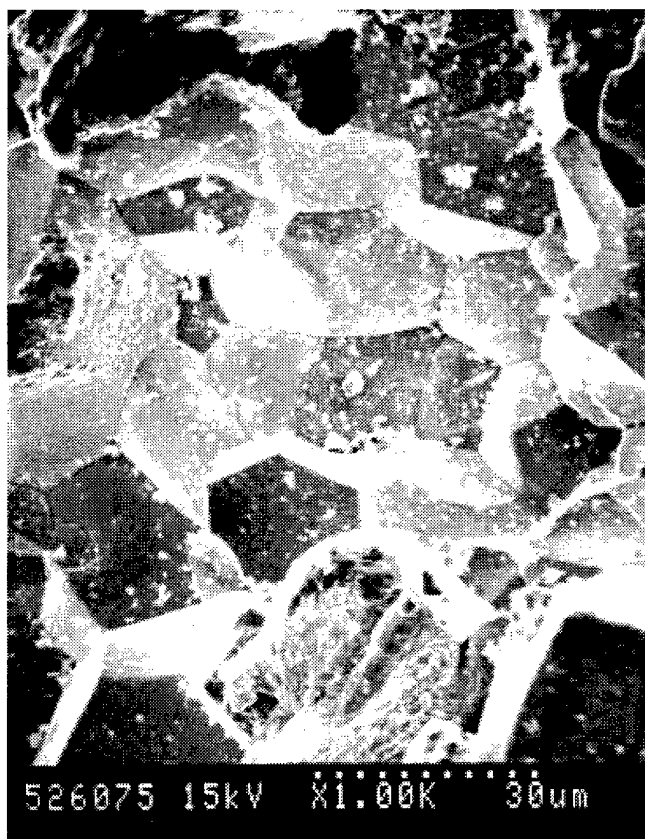
Figure 3. SEM micrograph of fracture surface of Pt-Ir wire fragment. Particles on surface are from the Ir/Al_2O_3 catalyst.

3

Figure 4. Photograph of four Pt-Ir wire fragments.

1.3   Mesh Processing and Motor Fabrication/Testing Review

The processing history of the 40 x 40 mesh screen, and the fabrication and acceptance testing of motor S/N KM004 were reviewed by Kaiser Marquardt and the prime contractor to identify potential causes of the wire failure. This review was greatly complicated by the fact that the thrust chamber assembly for this motor was built in 1990 by Hamilton Standard. Hamilton Standard subsequently discontinued this business, and the thrust chamber assembly on S/N KM004 was purchased by the government and supplied to Kaiser Marquardt as government-supplied equipment. Thus, it was difficult to obtain detailed information on Hamilton Standard's discontinued manufacturing processes.

Key processes in the fabrication of the retainer/screen assemblies are vacuum oven brazing at 1150°C (2100°F) of the screens to the retainer ring, gold plating of the braze, and cleaning of the screens throughout the manufacturing processes. Build records did not show any anomalies during the entire build process. The records also showed that the screen material for S/N KM004 was from a different lot than all other motors. The screen mesh was purchased from Johnson Mathey and was fabricated from lot number 94634 of Pt-15wt%-Ir wire. The 0.010- and 0.017-in.-diam wires were both from this lot.

A chemical analysis for detection of impurities in the wire lot was provided by Johnson Mathey and is shown in Table 1 along with the analysis of two other lots, which will be discussed below. The primary impurities in all three lots were Pd and Rh, which are Pt-group metals commonly present in Pt alloys and having no embrittling effect on Pt-Ir alloys. Elements known to have an embrittling effect such as Si, Ag, and Pb were either present in very low levels or were not detected in the three lots.

4

Table 1. Chemical Analyses Supplied by Manufacturers of Pt-15wt%-Ir Wire Lots

Element	Concentration, wt ppm			Element	Concentration, wt ppm		
	KM004 Lot	Lot No. 1	Lot No. 2		KM004 Lot	Lot No. 1	Lot No. 2
Pt	Major	84.90%	84.90%	Pb	ND	<10	<10
Pd	215	30	20	Sn	ND	NA	NA
Rh	213	20	20	Cr	15	NA	NA
Ir	Major	15.05%	15.06%	Si	5	<10	<10
Ru	ND	ND	ND	Fe	36	10	<5
Os	ND	NA	NA	Bi	ND	NA	NA
Au	20	20	10	Mo	ND	NA	NA
Ag	3	<2	<2	Cu	5	<5	<5
Cd	ND	NA	NA	Zn	ND	NA	NA
As	ND	NA	NA	Ti	ND	NA	NA
Te	ND	NA	NA	Co	ND	NA	NA
B	2	NA	NA	Ni	ND	5	<1
Sb	ND	NA	NA	Al	ND	NA	NA
Mn	ND	NA	NA	Ca	1	NA	NA
Mg	ND	<1	<1	Zr	ND	NA	NA

ND = Not detected
NA = Not included in analysis report

The only process identified as a potential source of silicon contamination was the hydroforming operation to form the dimples on the end screens. "Heavy-duty drawing oil" is used as a lubricant in the hydroforming process. Three vendor/product trade names for drawing oil were International Chemical/I. C. 484-S, Houghton Oil/E. P. 520, and Whitefield Richards/Lube-a-Tube. There was some concern that these products could contain silicones, which would be a possible source of Si contamination. M. R. Hilton[6] contacted the three vendors and determined that none of these products were intentionally fabricated with Si-containing additives. The vendors did caution, however, that silicon-containing anti-foaming agents are often used in cleaning fluids for oil removal. An aqueous cleaning solution was used by Hamilton Standard following hydroforming. Unfortunately, the chemistry of this solution has not been determined. However, once it was determined that the embrittled wire was within the mid-retainer/screen assembly, this became an irrelevant issue. The mid-screens are hand formed into the concave geometry. The drawing oils and aqueous cleaning solution are not employed on the mid screens.

The only known unique anomaly associated with the processing, fabrication, and testing of motor S/N 004 was a power failure during thermal vacuum testing at Kaiser Marquardt.[1] This power failure resulted in a back-flow of silicone diffusion pump oil into the vacuum chamber. Although no evidence of oil was found inside the REM, it was flushed with alcohol and four 100-ml catches were examined by Fourier-Transform Infrared (FTIR) spectroscopy. The FTIR revealed that there was no silicone oil present. Thus, the thermal vacuum test was repeated and successfully completed. Although FTIR did not reveal the presence of any silicone oil, for the purpose of this investigation, it was assumed that some contamination occurred. Thermal vacuum testing is performed following test firing so that the maximum temperature that the motor saw following silicone exposure was 191°C (375°F) in the thermal vacuum test. Breakdown of the silicone oil and diffusion of silicon

into the Pt-Ir wire is unlikely at such low temperatures. Nevertheless, considering the embrittling potential of Si and the observation of Si on the fracture surfaces, further investigation into the effects of this contamination on the wire screen was warranted.

1.4   Preliminary Simulation Experiments at Kaiser Marquardt

Pt-15wt%-Ir screen material from a different lot (designated Lot No. 1 by Kaiser Marquardt) and a different wire manufacturer (Sigmund Cohn Corp.) than that used in motor S/N KM004 was dipped in Dow Corning 704 diffusion pump oil and then exposed to one of two thermal treatments. One sample was exposed to 93°C (200°F) in vacuum for 4 h followed by a 180° crimping bend test at room temperature. The wire did not fracture, indicating that embrittlement did not occur. A second sample was exposed to 871°C (1600°F) for 20 min in an argon atmosphere, and was subsequently bent to a 90° angle and then tensile tested to failure at room temperature. This sample had a ductile failure, further suggesting that diffusion pump oil contamination did not cause the wire embrittlement.

A second lot of screen material, designated Lot No. 2 by Kaiser Marquardt, and also produced by Sigmund Cohn Corp., was used for grain size studies. Optical microscopy indicated that the Lot 2 wire had an ASTM grain size smaller than No. 8, corresponding to an average grain diameter of less than 20 μm. Thus, this material had a much finer grain size than the failed wire from motor S/N KM004. This observation opened the possibility that the unusually large grain size of the failed wire was a unique characteristic of this lot, which may have contributed to the embrittlement. However, the Kaiser Marquardt screen material was in the as-received condition, whereas the failed screen had been subjected to the high-temperature brazing process and several test firings. Thus, the Kaiser Marquardt screen material was exposed to a vacuum anneal at approximately 1150°C (2100°F) for 2 h to simulate the brazing process. After this heat treatment, the Kaiser Marquardt screen had an approximate grain size of ASTM No. 6, in the same size range as the failed screen. Thus, it was concluded that the large grain size of the failed screen was not a unique characteristic of this lot. Although the large grain size may have contributed to the embrittlement, it probably was not the primary cause.

2. Laboratory Analyses at The Aerospace Corporation

It has been well established that platinum alloys are susceptible to embrittlement by very low concentrations of elements such as Si, Ag, K, Pb, and Se that form low-melting-point phases at the grain boundaries.[1,7] Secondary-Ion Mass Spectroscopy (SIMS) has a higher sensitivity for detection of trace elements than do SEM/EDX or AES. Thus, it was concluded that the Cameca Ion Microprobe within the Mechanics and Materials Technology Center (MMTC) could provide additional chemical analysis data to supplement the EDX and AES data provided by the spacecraft contractor. Initially, four of the small wire fragments from the nozzle bag were provided to MMTC for analysis. These wire fragments were studied using SEM/EDX as an independent evaluation of the fracture surfaces, and were subsequently analyzed by SIMS. The initial plan was to perform SIMS on the fracture surfaces to directly detect any trace elements that may have contributed to the embrittlement of the grain boundaries. However, it was determined that the surface roughness generated by the multiple facets of the brittle fracture would not allow sufficient detection of the secondary ions to perform an analysis on the fracture surfaces. Therefore, one of the wire fragments was mounted and polished for SIMS analysis of a cross section parallel to the wire axis. This allowed analyses to be performed on areas immediately behind the fracture surface or far removed from the fracture.

After the motor was disassembled, additional material from the mid-retainer/screen assembly was provided to MMTC for evaluation. Photographs of the front and rear surfaces of the mid-retainer/screen assembly are shown in Figure 5. The top photograph shows a circular pattern of damage to the first 40 x 40 screen due to embrittlement of the 0.010-in.-diam wires. The lower photograph shows that the 18 x 18 mesh of 0.017-in.-diam wires was undamaged. The contractor sectioned the mid-retainer/screen assembly into quadrants by cutting along the lines shown in the upper photograph and sent Quadrant No. 2 to MMTC for evaluation.

The photograph in Figure 6 shows the damaged areas on Quadrant No. 2 and the cutting pattern for removing smaller samples for various evaluations and experiments. For the purpose of convenient sample identification, the top, brittle screen was identified as Mesh A, the middle screen as Mesh B, and the lower, coarse screen as Mesh C. Initially, the entire quadrant was evaluated using SEM/EDX to document fracture features and conduct preliminary chemical analyses of the wire surfaces and fracture surfaces. The quadrant was then sectioned as shown in Figure 6 using a low-speed diamond saw with deionized water as a lubricant. Samples A1, A2, and B1 were mounted and polished for performing SIMS analyses on wire cross sections. These samples were selected to allow comparisons between areas on Mesh A with and without brittle failures (A1 and A2, respectively) and to compare the damaged Mesh A with the apparently undamaged Mesh B. Samples A3, B3, and C3 were used for SIMS analyses of the wire surfaces. The intent of these analyses was not only to compare the surface chemistry for the three screens, but to also make comparisons between the "high points" (tensile side) of the wires at crossovers in the weave to the "saddle points" (compressive side) where the crossing wires contact one another. The high points can easily be contaminated during handling of the screens, whereas the saddle points are somewhat protected from contamination.
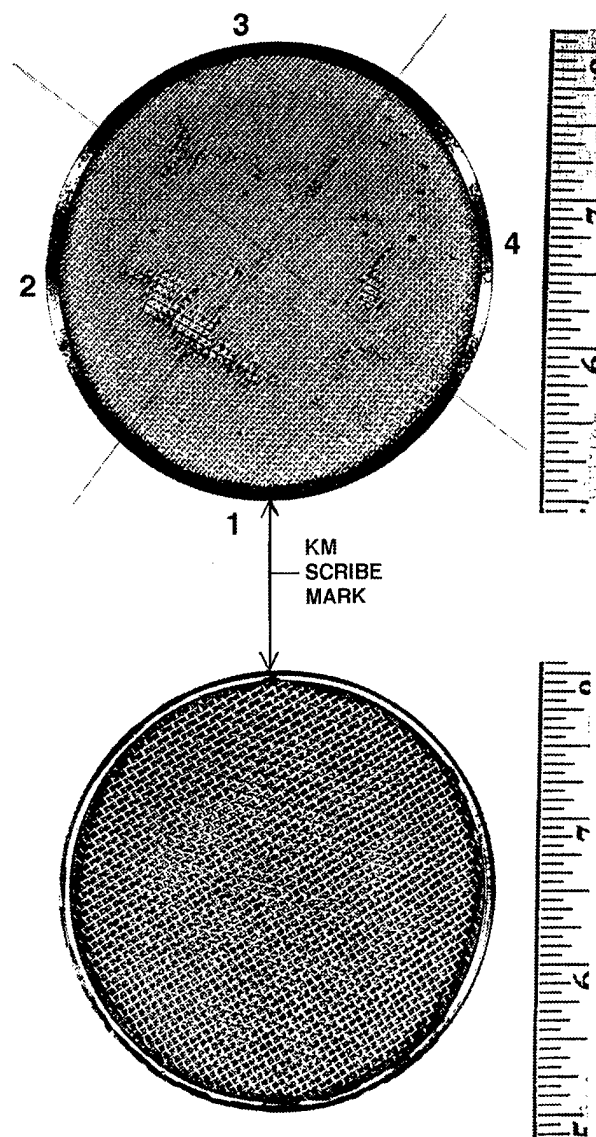
Figure 5. Photograph of up stream (top) and down stream (bottom) sides of mid-retainer/screen assembly. Top photograph shows location of cuts for sectioning into quadrants.
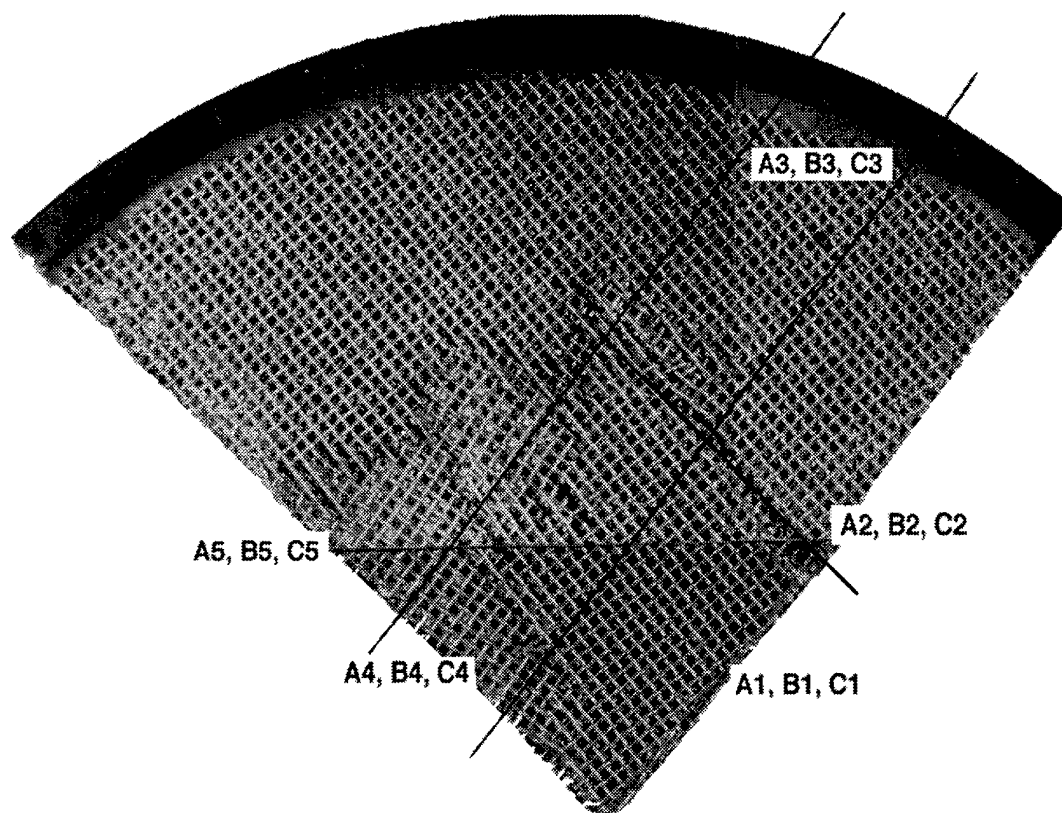
Figure 6. Photograph of Quadrant No. 2 from Mid-Retainer/Screen Assembly. The Screens Were Sectioned into Samples and Identified as Shown. Mesh A = Top, Embrittled Screen, Mesh B = Middle Screen, and Mesh C = Bottom Screen.

In order to prepare Samples A3, B3, and C3 for the SIMS surface analyses, it was necessary to extract one or two wires from each sample in order to expose the saddle points. It was anticipated that great care would be required in handling the presumably brittle Mesh A during the wire extraction process. However, it was discovered that considerable bending of the wires was possible without brittle fracture occurring. In some instances, wires were bent nearly 180° without cracking or fracturing. It was also discovered during the wire extraction process that the wires were difficult to separate at the crossover points. Initially, it was assumed that this was due to mechanical locking from the woven wire. However, even when the wires were bent straight, separation was difficult, and there appeared to be partial fusion between the wires at the saddle points.

In view of the surprising fracture resistance of the Mesh A wires during handling, it was hypothesized that the wires might be ductile at room temperature, but brittle at the firing temperature. Therefore, individual wires 0.50–0.75-in. long were extracted from Mesh A and Mesh B for the purpose of determining the tensile fracture mode at temperatures from 23 to 950°C (73 to 1740°F). These wires were extracted from the quadrant edge labeled A5, B5, C5 in Figure 6. The simple apparatus shown in Figure 7 was constructed to manually fracture the short wires in tension in a tube furnace. The elevated-temperature tensile fractures were created in an air atmosphere. Extracted wires were also used to perform various contamination experiments, which will be discussed below.

9

Furnace: 12-in. heat zone

20-in.-long by 0.375-in.-square rod
secured at left end to 38-in.-long by 0.5-
in.-square rod

Pt-Ir wire tightened under 0.25-in.-long screws
and fractured in tension by pulling unsecured
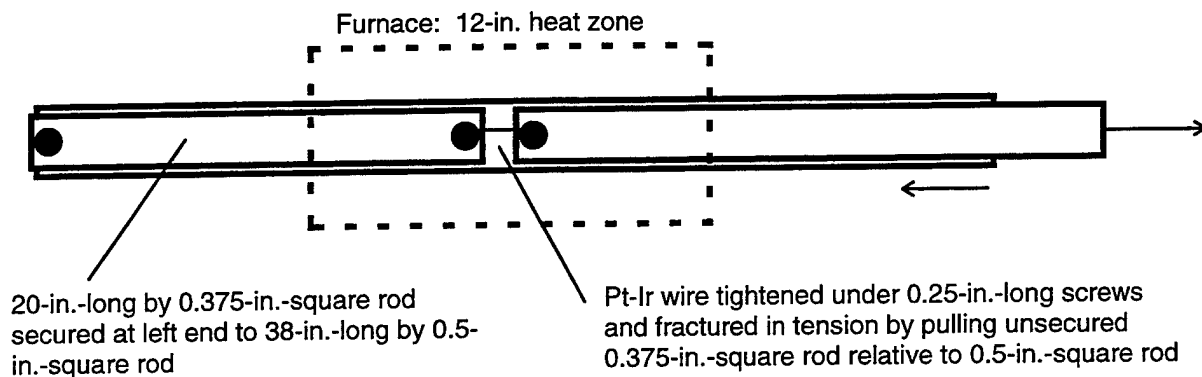0.375-in.-square rod relative to 0.5-in.-square rod

Figure 7.   Stainless-steel rod assembly for fracturing Pt-Ir wires in tension at high temperatures.

2.1   SEM/EDX of Wire Fragments

The micrograph in Figure 3 is from the SEM analysis of the wire fragments. The MMTC SEM/EDX results were completely consistent with those performed by the contractor. EDX was performed at several areas on fracture surfaces on two wire fragments such as that shown in Figure 3. In all cases, the only elements identified were Pt, Ir, Al, and O. No evidence of Si was detected. However, it should be noted that the Si K_α X-ray peak is located at an energy of 1.739 keV while the Pt and Ir M_α peaks are located at 2.048 keV and 1.977 keV, respectively. Thus, low concentrations of Si would be difficult to detect due to overlapping with the strong Pt and Ir peaks. Furthermore, EDX is not an effective technique for detection of thin layers of contaminants on material surfaces.

2.2   SEM/EDX of Quadrant No 2 of the Retainer/Screen Assembly

Extensive SEM/EDX analyses were conducted on the damaged areas of Quadrant No. 2. The primary objective of these analyses was to look for the presence of any contaminants that could have led to the embrittlement of Mesh A. Figure 8 shows a typical area from the damaged region. This figure shows four wires having brittle fractures, three wires oriented in one weave direction and one wire oriented in the other weave direction. Thus, the embrittlement did not appear to be associated with any preferential wire orientation within the screen. The Mesh B and Mesh C wires can be seen below the fractured Mesh A wires in the figure. The wires for all three screens had rough surfaces due to a high density of catalyst particles. EDX analyses at numerous locations on the wire surfaces revealed only Pt and Ir from the wires and Al, O, and Ir from the catalyst. A higher-magnification view of a cracked wire (Figure 9) shows the particles on the surface. This micrograph is typical of many cracked wires and shows the brittle, intergranular nature of the cracks. EDX analyses were also performed on the clean faces of these cracks just below the wire surface. These analyses usually revealed only Pt and Ir. Occasionally, Al and O were also detected, presumably from catalyst particles falling into the crevices.
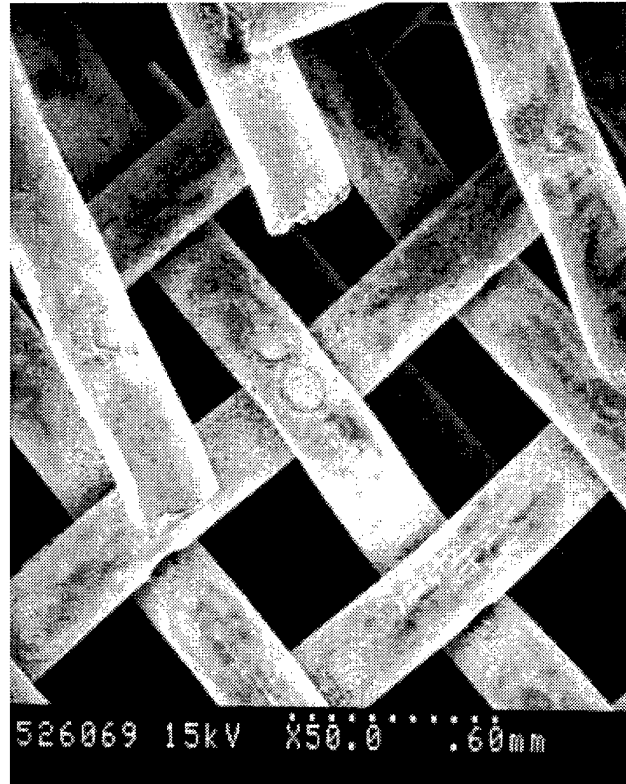
10

Figure 8. SEM micrograph of damaged area on mid-retainer/screen assembly.
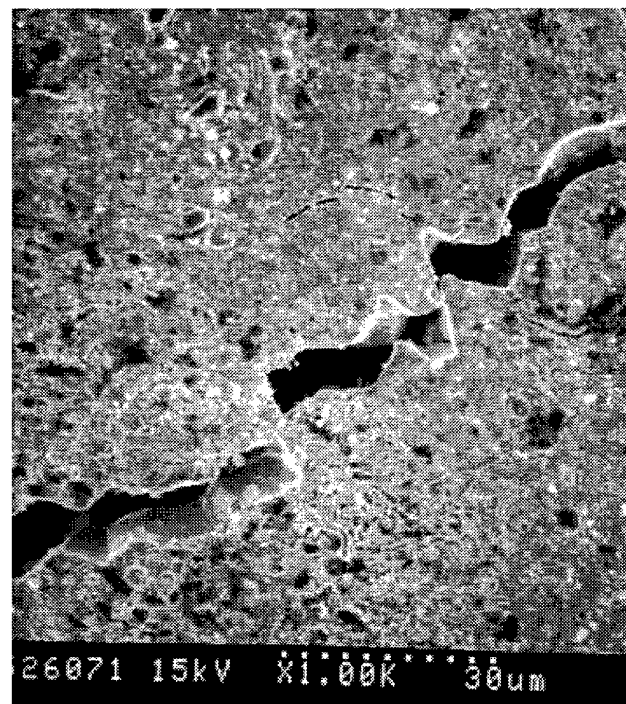

Figure 9. SEM micrograph of cracked Pt-Ir wire on Mesh A.

Figure 8 also shows that the wires underwent considerable deformation at the crossover points of the weave. The wire in the upper right corner of the figure appears to be slightly kinked within the saddle point of the crossover. This was a common observation. Figure 10a shows a higher magnification of a kinked saddle point. The saddle points were characterized by a reduced density of catalyst particles and considerable etching of the grain boundaries. Thermal etching of grain boundaries commonly occurs during high-temperature vacuum annealing (brazing operation), but may also occur in high-temperature reducing environments (motor firing). A higher-magnification view in Figure 10b demonstrates that in some areas, grains were completely dislodged. Other saddle points showed complete dissolution of the grain boundaries (Figure 11a), the development of voids at the grain boundaries (Figure 11b), or possible surface melting (Figure 11b). These observations are probably indicative of the embrittlement process and are contributors to the apparent partial fusion between crossing wires.

The saddle points shown in Figures 10 and 11 are from areas on Mesh A in which the saddle points were exposed when the crossing wire fractured. In order to view the saddle points on Meshes B and C, it was necessary to extract the crossing wire. Figure 12 shows a saddle point on Mesh C, which has the appearance of a ductile fracture surface. This fracture surface is direct evidence that the crossing wires were fused together. Figure 12 is typical of all saddle points (4 or 5) examined in the SEM for Mesh C. A larger number of saddle points was examined on Mesh B. Most of the Mesh B saddle points had the ductile fracture surface characteristic of the separation of fused wires over part of the crossover area and the "free surface" features shown in Figures 10 and 11 over the remainder of the area.

(a)   (b)
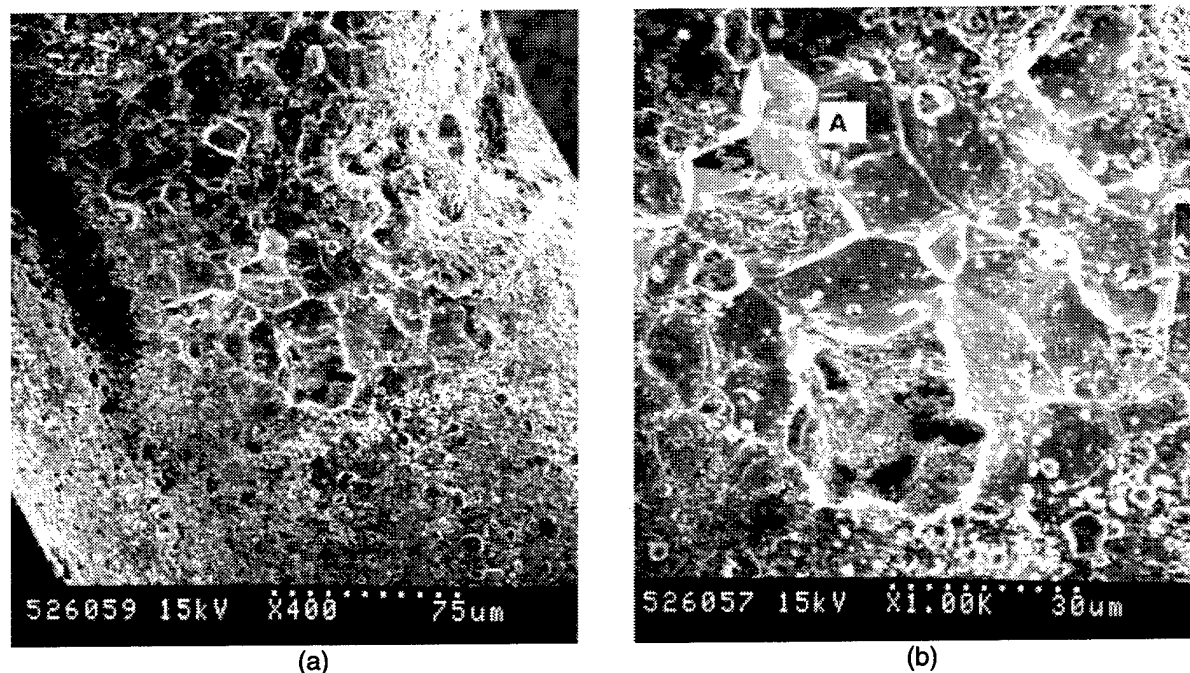
Figure 10.   SEM micrographs of a saddle point of a crossover point on Mesh A. The higher-magnification micrograph (b) shows dislodged grains at point A.

12

(a)   (b)

Figure 11. SEM micrographs of two saddle points at crossover points on Mesh A. Extensive grain boundary dissolution is shown in (a). Grain boundary voids along with possible melting at location A are shown in (b).
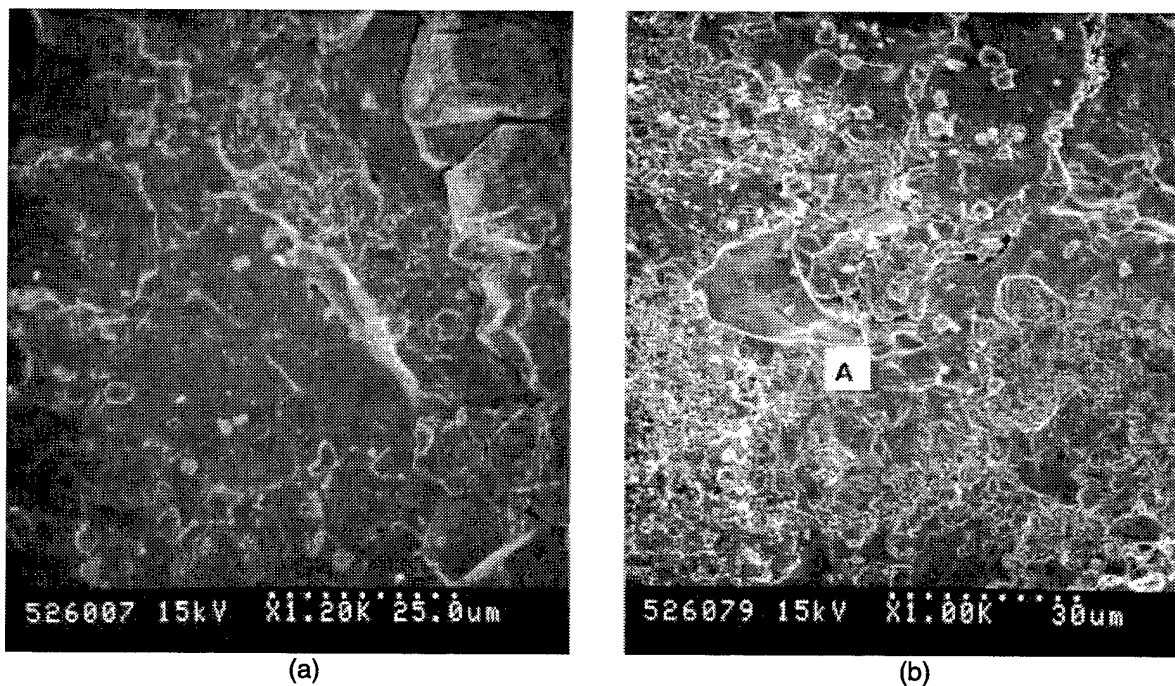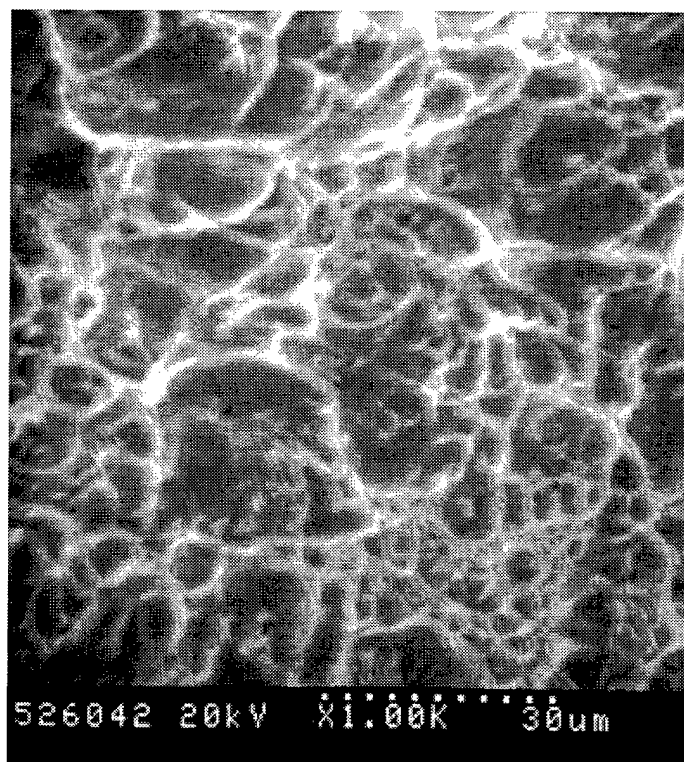

Figure 12. SEM micrograph of a saddle point of a crossover point on Mesh C.

13

2.3 Secondary-Ion Microprobe Spectroscopy (SIMS)

The SIMS analyses were performed using a Cameca IMS5f ion microprobe, a magnetic sector instrument. SIMS provides an elemental analysis of solid materials and can detect all elements from hydrogen through uranium. It is a highly sensitive technique capable of detecting many elements at very low concentrations. Quantification is difficult due to a very wide range of elemental sensitivities, and element concentration is not directly related to secondary-ion counts. For example, Pt is a noble metal that is very difficult to ionize. Thus, a low fraction of Pt atoms removed from the surface is ionized and counted. Therefore, in the present analyses, several impurities frequently had secondary-ion counts higher than the number of Pt ions counted, even though Pt was the host material.

For these analyses, a duoplasmatron source was used to obtain oxygen ions for the primary ion beam. Oxygen is used to enhance the secondary-ion yield of the electro-positive elements. A finely focused primary-ion beam of O_2^- ions accelerated to +12.5 kV was generated and rastered over a 100 x 100 μm analysis area on the surface of the sample. The sample was biased to +4.5 kV, giving a net acceleration voltage of 8.0 kV. The polarity of the secondary analyzer was set to detect positive secondary ions.

The mass spectra were obtained by sweeping the secondary magnet magnetic field from mass 1 to mass 250. Secondary ions of the elements at or near the surface pass through the secondary column and strike the secondary-ion detector. The output of the detector, an electron multiplier, is plotted as secondary-ion counts versus mass-to-charge ratio. This secondary-ion spectrum is used to determine the elements present in the region scanned by the primary-ion beam. Elemental maps were obtained by adjusting the secondary magnet to an element of interest and rastering the surface of the sample with the primary-ion beam.

For all spectra analyzed in this investigation, the number of secondary-ion counts for each species of interest was divided by the Pt secondary-ion count in order to allow semiquantitative comparisons between different spectra on a sample or between different samples. Some elements, such as Na or K that are common surface contaminants that are not known to embrittle Pt alloys and were found to rapidly decay during depth profiling, were disregarded. The oxygen peak was not considered in the analyses since an oxygen-ion beam was used.

Initially, SIMS was performed on cross sections of mounted and polished samples. One of the wire fragments from the nozzle bag was analyzed, followed by two mounted and polished cross sections of the Lot No. 2 screen material provided by Kaiser Marquardt. One of the Lot No. 2 samples was in the as-received condition, and the other was after the heat treatment simulating the braze process. After the motor was disassembled, two pieces from Mesh A (A1 from the damaged area and A2 from an undamaged area) and one piece from Mesh B (B1 from directly below A1) were mounted and polished for analysis. The Lot No. 2 samples were etched at Kaiser Marquardt, while the samples prepared at Aerospace were unetched. All of the mounted samples were coated with a thin layer of gold in order to electrically ground the sample during analysis.

The results of the spectral analyses of the cross sections are shown in Table 2. The numbers of secondary-ion counts are given in the top of the table, and the ion count ratios relative to Pt are given in the bottom of the table and in the bar chart in Figure 13. The atomic mass for the peak used for the ion

Table 2. Summary of SIMS Spectra for Cross Sections of Pt-Ir Wire Fragment and Mesh A, Mesh B, and Lot No. 2 Screens

ELEMENT OR COMPOUND	SECONDARY ION COUNTS FOR SAMPLE NO.							
	WIRE FRAGMENT	A1, AREA A	A1, AREA B	A2, AREA A	A2, AREA B	B1, AREA A	KAISER MOUNT No. 15166 = LOT No. 2, AS-RECEIVED	KAISER MOUNT No. 15169 = LOT No. 2, BRAZE HEAT TREATMENT
Si (28)	1100	1200	5000	1500	650	550	25	150
Ca (40)	510	9100	5000	4500	3000	1700	19	490
In (115)	1000	1300	2200	2100	2500	2000	42	45
Pt (195)	1400	1700	2000	2200	2100	2000	600	700
Ga (69)	100	70	50	120	120	30	30	9
Mn (55)	60	100	80	100	130	90	28000	25000
Cr (52)	1100	1200	910	1000	1000	950	85	100
Al (27)	620	740	900	820	2100	650	16	100
Cu (63)	59	190	120	100	100	120	10	21
SECONDARY ION COUNT RATIOS								
Si/Pt	0.79	0.71	2.50	0.68	0.31	0.28	0.04	0.21
Ca/Pt	0.36	5.35	2.50	2.05	1.43	0.85	0.03	0.70
In/Pt	0.71	0.76	1.10	0.95	1.19	1.00	0.07	0.06
Ga/Pt	0.07	0.04	0.03	0.05	0.06	0.02	0.05	0.01
Mn/Pt	0.04	0.06	0.04	0.05	0.06	0.05	46.67	35.71
Cr/Pt	0.79	0.71	0.46	0.45	0.48	0.48	0.14	0.14
Al/Pt	0.44	0.44	0.45	0.37	1.00	0.33	0.03	0.14
Cu/Pt	0.04	0.11	0.06	0.05	0.05	0.06	0.02	0.03

counts is indicated in parentheses for each element or compound. Spectral data are presented for two separate areas on Sample Nos. A1 and A2, and for one area on all other samples. Similar elemental spectra were obtained for the wire fragment, the two areas on Sample Nos. A1 and A2, and the one area on Sample No. B1. The primary impurities were Cr, Rh, Al, In, Si, and Ca. Rh was not included in Table 2 or Figure 13 since the presence of Rh is expected and is of no concern. Indium was the most surprising impurity and appeared to be present in significant levels, although not at concentrations sufficient to be detected by SEM/EDX. Cr, Rh, Si, and Ca were all detected in the bulk chemical analysis (Table 1), while Al was not detected, and In was not checked for in the bulk analysis. Elemental mapping indicated that the Cr, Rh, Al, and In were distributed uniformly throughout the cross section. The Ca and Si were associated with one another and appeared to be present as distinct particles, as shown by the elemental maps in Figure 14 for Sample No. A2, Area B.
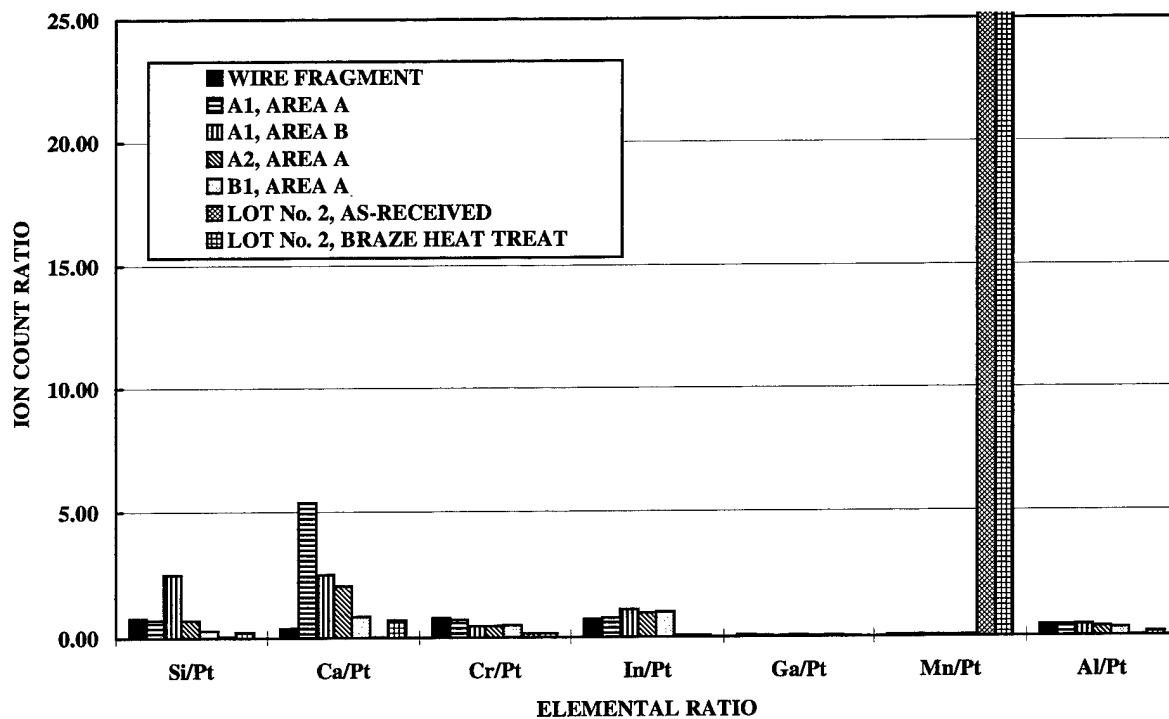
Figure 13. Primary impurities detected in SIMS analysis of cross sections of Pt-Ir wire fragment and Mesh A, Mesh B, and Lot No. 2 screens.
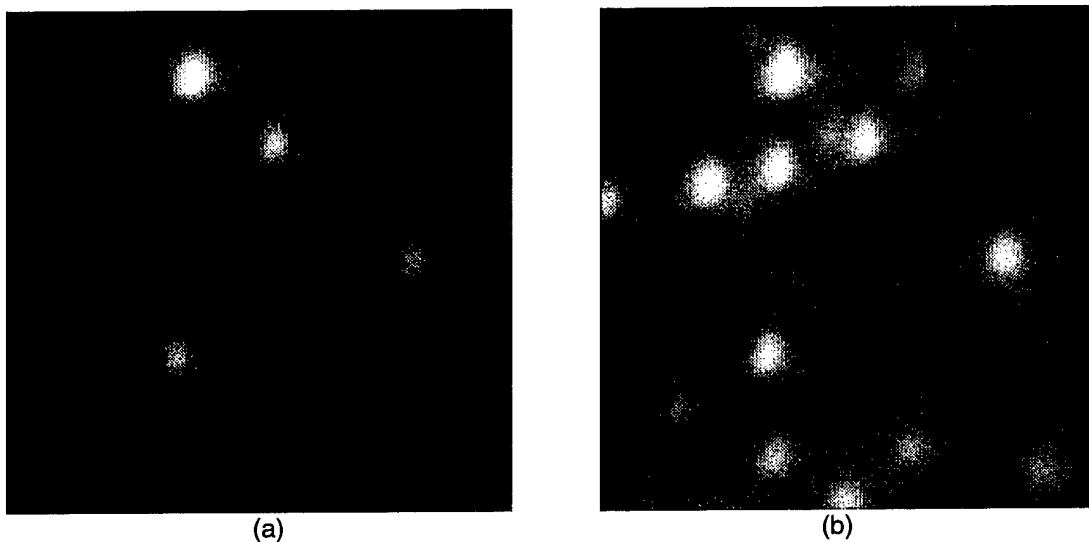

Figure 14. Silicon (a) and calcium (b) Maps of analysis Area B on cross section of Sample No. A2. Bright spots indicate presence of Si or Ca.

16

Initially, there was some concern that the Si- and Ca-rich particles might be contamination from the SiC abrasive paper used in the sample grinding operation. However, additional mapping indicated that there was no carbon associated with the particles. Furthermore, it was discovered that during depth profiling, some of the particles were sputtered away while new particles appeared at different points. Thus, it was concluded that the particles were present within the bulk of the samples and were not a sample preparation artifact. The relative spatial positioning of the particles, as demonstrated by the Ca map in Figure 14, suggested that the particles could be located at the grain boundaries. Unfortunately, the magnification (70x) of the optical microscope on the microprobe was not adequate to sufficiently resolve the grain structure to make any correlation between the relative locations of the grain boundaries and the Ca-Si particles. However, the ion beam does etch the sample over the 100-μm analysis area. Therefore, the analysis area could subsequently be identified with the SEM and is shown in Figure 15. EDX analyses indicated that most of the dark spots in Figure 15 are composed of Ca, Si, and O. The other dark spots appear to be voids left behind by dislodged particles. These particles are assumed to be the same as shown in Figure 14, and some correlation in the location of the particles can be seen when comparing the two figures. The most significant observation from Figure 15 is that most of the Ca-Si-O particles are located within the grains rather than at the grain boundaries. For this reason, it was concluded that these particles probably did not cause the embrittlement of Mesh A. This conclusion was further supported by the fact that the particles were not only observed by SIMS mapping on all Mesh A samples, but were also present on Mesh B (Sample B2), which showed no evidence of embrittlement.
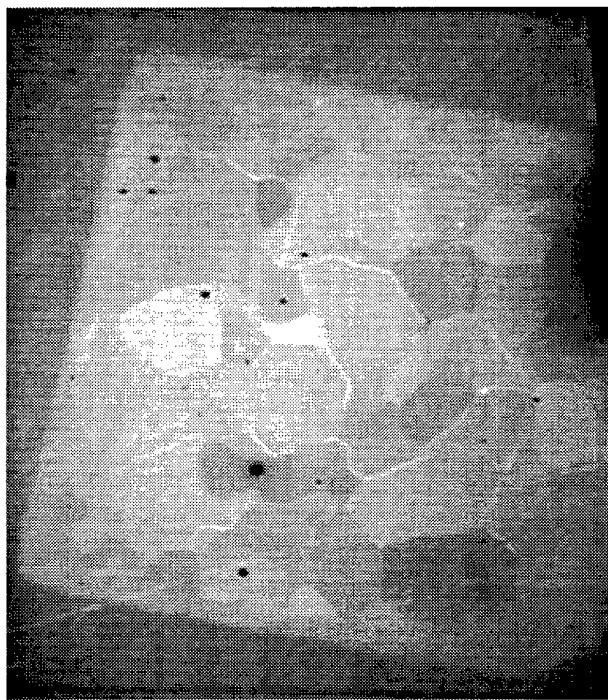

Figure 15. SEM Micrograph of Area B on Sample No. A2 following SIMS analysis. EDX analysis indicated that dark spots are Ca-Si-O particles.

17

The SIMS analysis of cross sections did not reveal any significant differences between the wire fragment and Sample Nos. A1, A2, or B1. The results were consistent with the fact that all of these samples were from the same lot of Pt-15wt%-Ir wire. The Lot No. 2 material had reduced levels of impurities compared to the samples from S/N KM004. The only significant impurity was Mn, which had a very high Mn/Pt peak ratio. The bulk Mn concentration was not listed in Table 1 and may not have been included in the analysis. There were no significant differences between the as-received and heat-treated samples for Lot No. 2.

Once it was determined that the SIMS analysis of cross sections did not identify any cause for the wire embrittlement, samples from each of the three screens were prepared for surface analyses. The results for Sample No. A3 will be presented first, followed by results for Sample Nos. B3 and C3. The results of the spectral analyses for Sample No. A3 are presented in Table 3 and by the bar chart in Figure 16. Four areas were analyzed, including two high points that had cracks completely across

Table 3. Summary of SIMS Spectra for Surfaces of Pt-Ir Screen Sample No. A3.

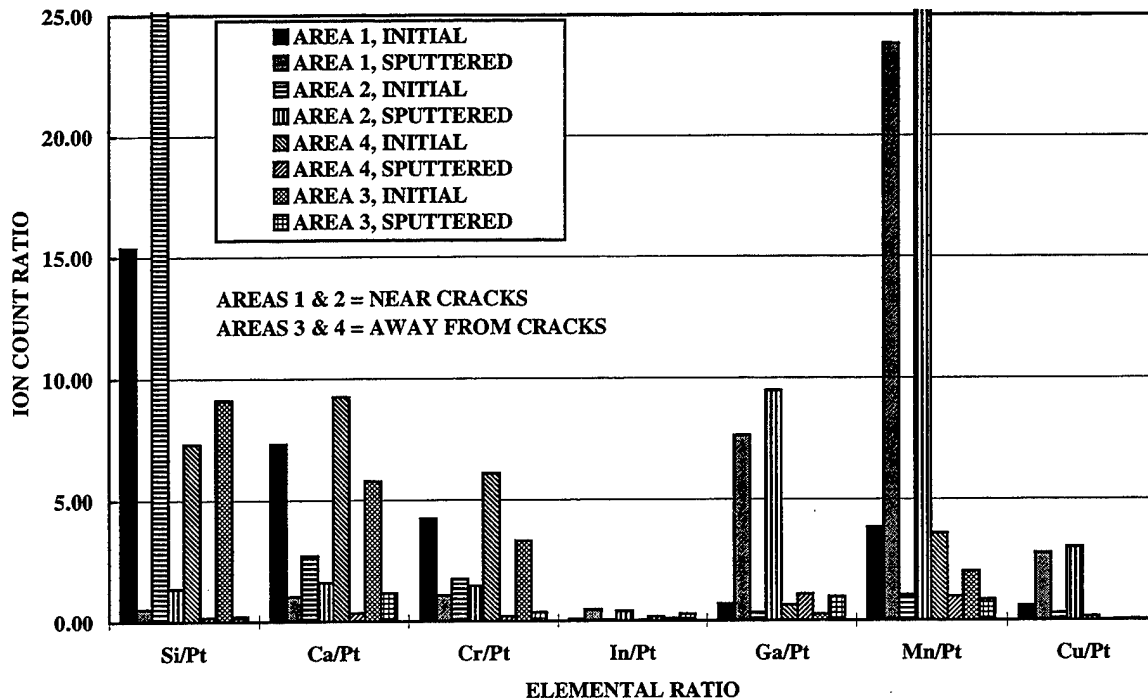| ELEMENT OR COMPOUND	SECONDARY ION COUNTS FOR SAMPLE NUMBER							
	A3, AREA 1, NEAR CRACK, INITIAL SCAN	A3, AREA 1, NEAR CRACK, SPUTTERED	A3, AREA 2, NEAR CRACK, INITIAL SCAN	A3, AREA 2, NEAR CRACK, SPUTTERED	A3, AREA 4, HIGH POINT (NEAR 1 & 2), INITIAL SCAN	A3, AREA 4, HIGH POINT (NEAR 1 & 2), SPUTTERED	A3, AREA 3, SADDLE POINT (AWAY FROM 1 & 2), INITIAL SCAN	A3, AREA 3, SADDLE POINT (AWAY FROM 1 & 2), SPUTTERED
Si (28)	2000	110	12000	260	950	18	710	25
Ca (40)	950	220	820	310	1200	34	450	130
In (115)	8	100	13	78	4	18	6	32
Pt (195)	130	210	300	190	130	100	78	110
Ga (69)	90	1600	100	1800	84	110	20	110
Mn (55)	500	5000	320	5000	470	100	160	95
Cr (52)	550	230	530	280	790	20	260	40
Al (27)	100000	12000	100000	22000	27000	5800	36000	16000
Cu (63)	80	590	90	580	21	0	2	4
SECONDARY ION COUNT RATIO								
Si/Pt	15.38	0.52	40.00	1.37	7.31	0.18	9.10	0.23
Ca/Pt	7.31	1.05	2.73	1.63	9.23	0.34	5.77	1.18
In/Pt	0.06	0.48	0.04	0.41	0.03	0.18	0.08	0.29
Ga/Pt	0.69	7.62	0.33	9.47	0.65	1.10	0.26	1.00
Mn/Pt	3.85	23.81	1.07	26.32	3.62	1.00	2.05	0.86
Cr/Pt	4.23	1.10	1.77	1.47	6.08	0.20	3.33	0.36
Al/Pt	769.23	57.14	333.33	115.79	207.69	58.00	461.54	145.45
Cu/Pt	0.62	2.81	0.30	3.05	0.16	0.00	0.03	0.04

Figure 16. Primary impurities detected in SIMS analysis of surfaces of Pt-Ir
screen sample No. A3.

the wire strands, one high point that did not have any cracks, and one saddle point. The areas ana-
lyzed on the cracked wires were adjacent to the cracks. Initial surface spectra were obtained at each
area followed by sputtering for up to 90 min. Additional spectra were taken after 30, 60, and 90 min
of sputtering. Results for the initial and final spectra will be discussed. The 30 and 60 min spectra
were either intermediate between the initial and final spectra or were very similar to the final spectra.

The two areas at high points adjacent to cracks (Areas 1 and 2) had similar results, which differed
from the points away from cracks (Areas 3 and 4). The surface spectra showed very high levels of
Si, which decreased rapidly during sputtering. Ca and Cr also decreased during sputtering. After the
90-min sputter, the Si, Ca, and Cr levels were similar to those for the cross-sectioned samples. There
were also low levels of In, Ga, Mn, and Cu on the surfaces at Areas 1 and 2. All of these elements
increased during sputtering. Ga and Mn showed the largest increases.

Results for the high point without any cracks (Area 4) and the saddle point (Area 3) were similar.
These areas had lower surface Si, but similar surface Ca and Cr compared to the high points near
cracks. All three elements decreased during sputtering and after 90 min were in the same ranges as
the sputtered high points near cracks and polished cross sections. In, Ga, Mn, and Cu were low on
the surfaces of the high point without cracks and saddle point and did not increase with sputtering.

19

All four areas had very large Al peaks from the alumina in the catalyst. Although the Al peak height decreased during sputtering, it was always the highest peak. Rh was also present at all four points and generally increased during sputtering.

Attempts at elemental mapping were not as successful as for polished cross sections. Most elements appeared to be distributed in the same areas. This may have been an effect of the artificial surface roughness created by the high density of alumina particles on the surfaces. It was not possible to distinguish whether a given element came from the Pt-Ir wire or whether it came from the catalyst particles. Therefore, a separate analysis was performed on the catalyst and will be discussed below.

The results for Sample Nos. B3 and C3 are presented in Table 4 and Figure 17. One high point and one saddle point were analyzed for both B3 and C3. Spectra were taken for the initial surfaces and

Table 4. Summary of SIMS Spectra on Surfaces of Pt-Ir Screen Sample Nos. B3 & C3

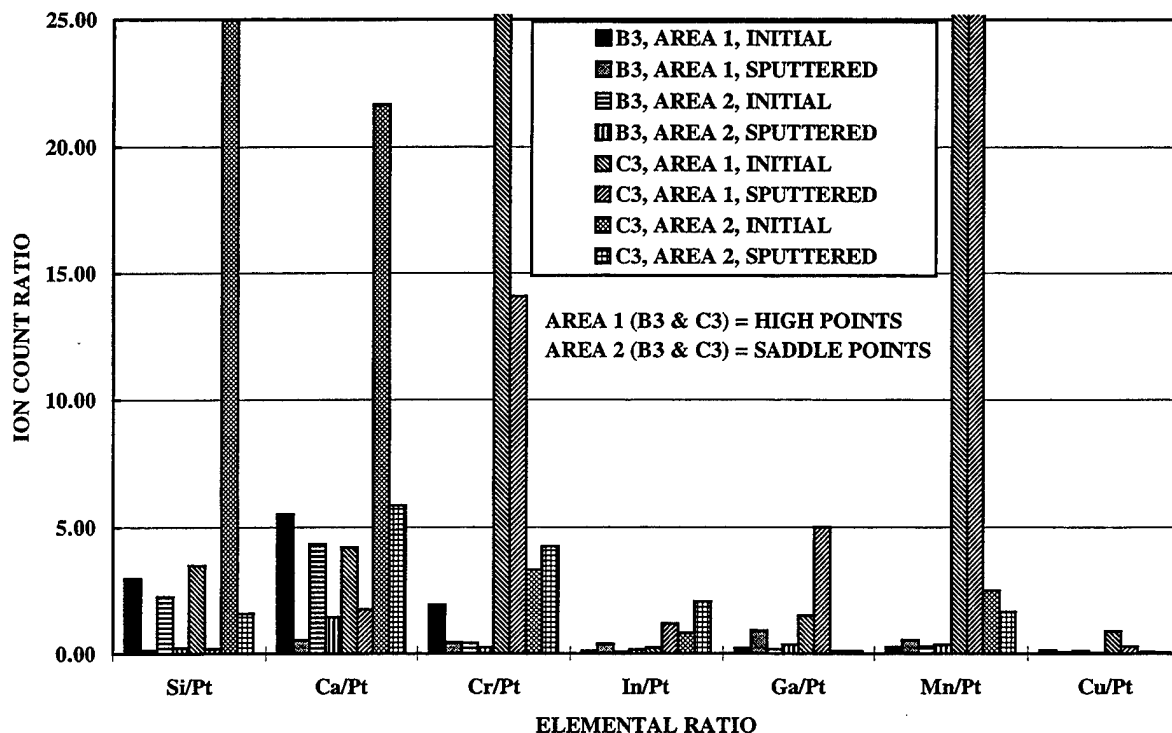| ELEMENT OR COMPOUND	SECONDARY ION COUNTS FOR SAMPLE NUMBER							
	B3, AREA 1, HIGH POINT, INITIAL SCAN	B3, AREA 1, HIGH POINT, SPUTTERED	B3, AREA 2, SADDLE POINT, INITIAL SCAN	B3, AREA 2, SADDLE POINT, SPUTTERED	C3, AREA 1, HIGH POINT, INITIAL SCAN	C3, AREA 1, HIGH POINT, SPUTTERED	C3, AREA 2, SADDLE POINT, INITIAL SCAN	C3, AREA 2, SADDLE POINT, SPUTTERED
Si (28)	1200	17	410	41	700	42	6000	190
Ca (40)	2200	70	780	250	840	390	5200	700
In (115)	42	50	11	25	45	260	200	250
Pt (195)	400	130	180	170	200	220	240	120
Ga (69)	89	120	29	60	300	1100	21	11
Mn (55)	100	70	48	60	5900	7000	600	200
Cr (52)	780	58	77	42	10000	3100	800	510
Al (27)	3800	100000	100000	100000	100000	20000	100000	100000
Cu (63)	55	5	18	4	180	60	16	5
SECONDARY ION COUNT RATIO								
Si/Pt	3.00	0.13	2.28	0.24	3.50	0.19	25.00	1.58
Ca/Pt	5.50	0.54	4.33	1.47	4.20	1.77	21.67	5.83
In/Pt	0.11	0.38	0.06	0.15	0.23	1.18	0.83	2.08
Ga/Pt	0.22	0.92	0.16	0.35	1.50	5.00	0.09	0.09
Mn/Pt	0.25	0.54	0.27	0.35	29.50	31.82	2.50	1.67
Cr/Pt	1.95	0.45	0.43	0.25	50.00	14.09	3.33	4.25
Al/Pt	9.50	769.23	555.56	588.24	500.00	90.91	416.67	833.33
Cu/Pt	0.14	0.04	0.10	0.02	0.90	0.27	0.07	0.04

Figure 17. Primary impurities detected in SIMS analysis of surfaces of Pt-Ir
screen sample Nos. B3 & C3.

after up to 90 min of sputtering. For Sample No. B3, similar results were obtained at the high point
and saddle point. Aside from Al from the catalyst particles, Si and Ca were the primary impurities
on the surface. Both decreased significantly during sputtering. There were only traces of In, Ga,
Mn, or Cu before or after sputtering.

Sample No. C3 had high Si and Ca on the surface at the saddle point. Si and Ca diminished during
sputtering, but remained somewhat higher than for Sample No. B3. This area also had higher Cr, In,
and Mn than for Sample No. B3 or for the polished cross sections.

The surface spectra for Sample No. C3 at the high point had Si and Ca levels similar to Sample No.
B3, but had very high levels of Cr and Mn. It also appeared to have more Ga present on the initial
surface than for any other sample. Ca and Si decreased during sputtering, while Cr and Mn remained
high, and In and Ga increased. Thus, following sputtering, the spectrum for this area was similar to
the areas near cracks on Sample No. A3.

The primary elements identified in the SIMS analysis of the catalyst bed sample were Al from the
alumina carrier and the Ir catalyst. Impurities were Si, Ca, and Cr. None of the other major impuri-
ties (Mn, Ga, and Cu) detected on the wire samples were present on the catalyst. Therefore, it would
appear that the only impurities on the screens that originated from the catalyst were the aluminum
oxide and Ir particles. The fact that Si and Ca were present on the surface of all areas analyzed sug-
gests that these impurities may have originated from the diffusion pump oil. The fact that the

21

secondary-ion counts for these elements quickly diminished during sputtering of the mesh samples is consistent with this conclusion. No sputtering of the catalyst sample was performed.

Sample Nos. A3, B3, and C3 were examined in the SEM following the SIMS analyses. Figure 18a shows Areas 1 and 2 from the SIMS analyses on Sample No. A3, and Figure 18b shows a higher-magnification view of Area 2. A comparison of Figure 18b with Figure 9 shows that the 90-min ion sputtering during the SIMS analysis cleaned a significant fraction of the catalyst particles from the wire surface and also etched the grain boundaries. Extensive EDX over the etched area did not reveal any elements other than Pt, Ir, Al, and O. Thus, although the Mn/Pt and Ga/Pt secondary-ion count ratios after sputtering were very high on Area 2 (Figure 16), the actual concentrations of Ga and Mn were too low to be detected by EDX.

The areas from the SIMS analysis were not immediately apparent on Sample No. C3. In the course of attempting to identify these points, a small intergranular crack was discovered on the tensile side of a wire at a crossover point in the weave. Thus, Mesh C was also embrittled, at least at one point. The 0.017-in.-diam wires in Mesh C were not as highly deformed as the 0.010-in.-diam wires in Meshes A & B. It is conceivable that Mesh C was embrittled to the same extent as Mesh A, but the tensile stresses at the bends were much lower than for Mesh A so extensive fracturing did not occur.
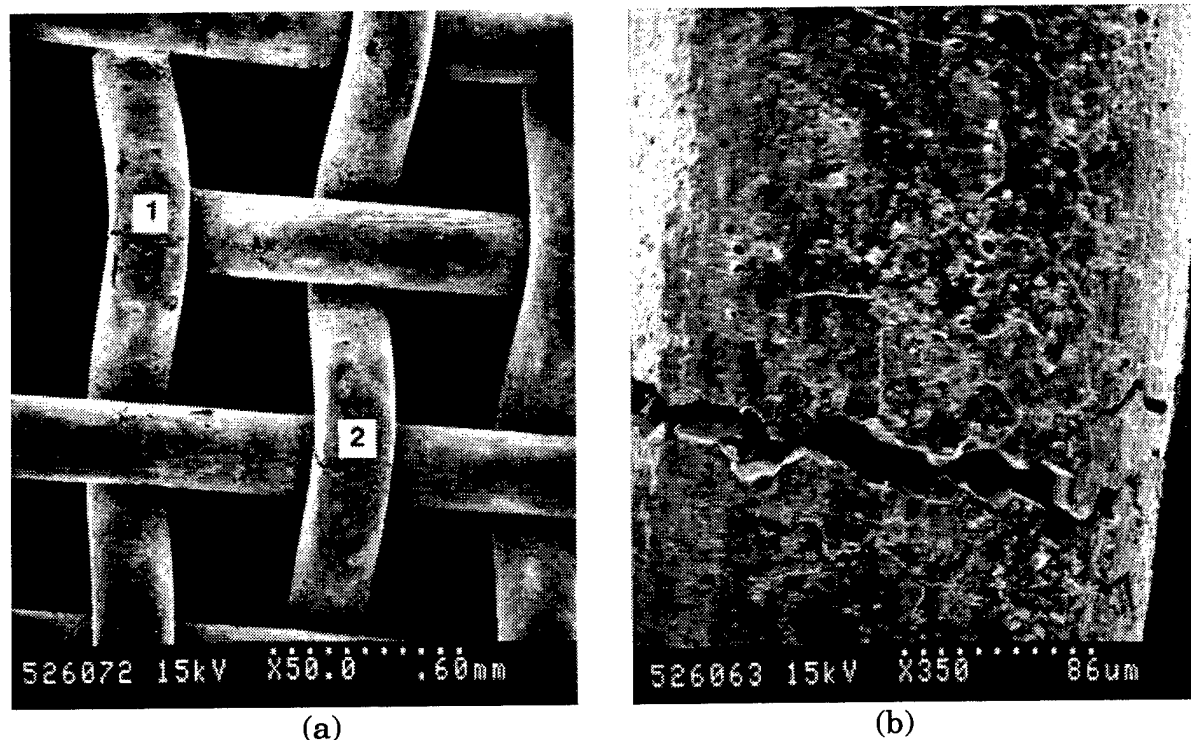

(a)   (b)

Figure 18. SEM micrographs of Sample No. A3 following SIMS analysis. Micrograph (a) shows Areas 1 & 2 adjacent to cracks. Micrograph (b) is higher-magnification view of Area 2.

2.4 Tensile Tests on Wires Extracted from Mesh A & Mesh B

The apparatus shown in Figure 7 was used to manually tensile fracture the 0.5–0.75-in.-long wires extracted from Mesh A and Mesh B. Wires extracted from Mesh A were pulled to failure at 23, 300, and 900°C (73, 570, and 1650°F) . Wires extracted from Mesh B were pulled to failure at 23, 850, and 950°C (73, 1560, and 1740°F). The tests were performed at 23°C because handling of Quadrant No. 2 indicated that Mesh A wires could be deformed much further at room temperature without fracturing than was anticipated. 300°C (570°F) was selected as a temperature somewhat higher than the maximum temperature, 190°C (375°F) that the REM was exposed to after potential exposure to diffusion pump oil. Tests were performed at 850–950°C (1560–1740°F) because these temperatures approach the maximum temperature, 980°C (1800°F) that the up stream screens were estimated to have seen during motor firing.

The wires extracted from both screens exhibited ductile fractures at room temperature. The wires from Mesh B also had ductile fractures at 850 and 950°C (1560 and 1740°F). The Mesh A wire pulled at 300°C (570°F) had a ductile fracture, but the wire pulled to failure at 900°C (1650°F) had a brittle, intergranular fracture with the same appearance as the fractures on the screen. Although a limited number of wires were fractured, these results suggest that the intergranular failures occurred at an elevated temperature, probably during motor firing. It is unlikely that contamination of the REM with diffusion pump oil embrittled the Pt-Ir wires since the temperatures that the REM saw after this contamination were not high enough to cause an intergranular failure. The fact that a Mesh A wire fractured in an intergranular mode at 900°C (1650°F) while Mesh B wires fractured in a ductile mode at 850 and 950°C (1560 and 1740°F), suggested that the Mesh B wires were not embrittled. This, of course, is consistent with the fact that no Mesh B fractures were observed on the up-stream retainer/screen assembly.

2.5 Gallium Contamination Experiments on Mesh B Wires

The SIMS analysis indicated the presence of much higher levels of Ga on wire surfaces adjacent to intergranular cracks than was observed at other locations. Ga is low-melting, 29°C (84°F), element that is known to cause liquid-metal embrittlement in some metals, including aluminum alloys, some steels, silver, and gold.[8] Therefore, a series of three experiments was performed in which extracted wires from Mesh B were contaminated with Ga in an effort to reproduce the intergranular fractures observed on Mesh A. In these experiments, 0.75-in.-long wires were bent into a 180° loop so that the center of the wire could be dipped in molten Ga without immersion of the wire ends. The wires were then exposed to 900–950°C (1650–1740°F) in an air atmosphere. In the first experiment, molten Ga was left on the wire surface during the elevated temperature exposure, and the sample was fractured in tension at room temperature following the exposure. In the other two experiments, the molten Ga was wiped from the surface before the elevated-temperature exposure, and the wires were pulled to failure at 900°C (1650°F). Although some degree of intergranular fracture was observed on these samples, they did not reproduce the fracture features observed on the Mesh A wires. The failure of these experiments to reproduce the wire failures does not dismiss Ga as a potential cause of the embrittlement. One major shortcoming of these experiments was that they did not reproduce the reducing atmosphere of the REM. The Ga layer on the samples was heavily oxidized after the high-temperature exposures. The presence of oxygen frequently disrupts liquid-metal embrittlement.[8] Furthermore, most embrittlement mechanisms for Pt alloys require a nonoxidizing environment.[2]

2.6   SEM Observations on Kaiser Marquardt Pt-Ir Screens

The Kaiser Marquardt Pt-Ir screens designated Lot Nos. 1 and 2 that were subjected to the braze simulation heat treatment were submitted to MMTC for evaluation. The primary goal was to determine whether these screens exhibited the partial fusion at weave crossover points that were observed for the screens from REM S/N KM004. Lot No. 1 was heat treated at 1150°C (2100°F) for 2 h to simulate the braze operation. Lot No. 2 was subjected to this heat treatment twice. Wires were extracted from both screens under a stereo microscope at a magnification of 20x. For both heat-treated lots, the wires were very easily extracted with no indications of fusion between wires. Figure 19 shows that the wires were subjected to substantial deformation at the crossover points, not unlike the deformation experienced by the wires in the S/N KM004 screens. However, the wires in the Lot No. 1 and 2 screens showed no evidence of the dislodged grains, dissolution of grain boundaries, voids at the grain boundaries, or fusion between wires seen on the embrittled wires.
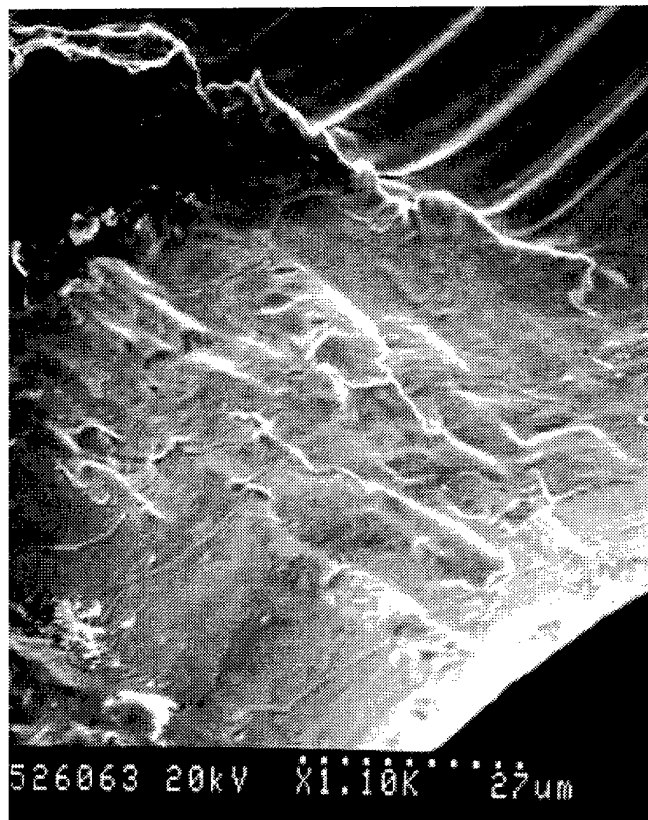

Figure 19.   SEM micrograph of a saddle point of a crossover
point on Kaiser Marquardt Lot No. 2 screen
following heat treatment simulating brazing.

24

3. Summary and Discussion of Failure Analysis Results

The goals of this failure investigation were to identify the cause of the embrittlement of the mid-screen on REM S/N KM004 and determine whether this failure would impact the flight worthiness of other Kaiser Marquardt and Hamilton Standard motors. Numerous significant facts relating to the failure and its implications on other flight motors were uncovered by the failure investigation team. These facts are as follows.

1. The up-stream screen on the mid-retainer/screen assembly of REM S/N KM004 suffered numerous brittle, intergranular fractures at bend points of the weave.

2. Silicon was detected on the tensile side of fracture surfaces using AES, but was not detected with EDX.

3. The thrust chamber on S/N KM004 was built by Hamilton Standard.

4. The Pt-15wt%-Ir wire used on the mid-retainer/screen assembly was a unique lot that was not used on any other Hamilton Standard or Kaiser Marquardt REMs.

5. The Pt-15wt%-Ir wire used on Hamilton Standard thrust chambers was produced and woven into screens by Johnson Mathey. The Pt-15wt%-Ir wire used on all Kaiser Marquardt thrust chambers was produced by Sigmund Cohn Corp. and was woven into screens by Unique Wire Weaving.

6. REM S/N KM004 may have been exposed to silicone diffusion pump oil during thermal vacuum testing. The maximum temperature that the REM was exposed to following this incident was 191°C (375°F). Kaiser Marquardt performed experiments to simulate the diffusion pump oil exposure and the subsequent thermal history. These experiments did not result in embrittlement of Pt-15wt%-Ir screens.

7. The Pt-15wt%-Ir wire from the S/N KM004 mid-screens had a much larger grain size than the as-received screens in Kaiser Marquardt's inventory. However, after the Kaiser Marquardt wire was subjected to a heat treatment simulating the brazing operation, it had a grain size in the same ASTM size range as the KM004 mid-screens. Thus, it was determined that the large grain size was not a unique characteristic of the lot of wire used in the KM004 mid screens.

8. The process of extracting wires from the fractured screen revealed that considerable bending of the wires was possible at room temperature without brittle fracture occurring. Furthermore, wires extracted from Meshes A and B exhibited a ductile fracture mode when pulled to failure at room temperature.

9. A wire extracted from Mesh A reproduced the brittle, intergranular fracture features of the failed screen when pulled to failure at 900°C (1650°F).

10. A wire extracted from Mesh A exhibited a ductile fracture mode when pulled to failure at 300°C (570°F). Wires extracted from Mesh B fractured in a ductile mode when pulled to failure at 850 or 950°C (1560 or 1650°F).

11. The process of extracting wires from all three screens of the mid-retainer/screen assembly revealed that it was difficult to separate wires at the crossover points. SEM showed ductile fracture characteristics at many crossover points after the wires were pulled apart. It was concluded that the wires were partially fused together at the crossover points.

12. SEM revealed that in addition to partial fusion, the saddle point of the wire crossovers on Meshes A and B were characterized by considerable etching of the grain boundaries. In some cases, large voids at the grain boundaries, complete dissolution of the grain boundaries, or dislodging of grains was observed.

13. The extraction of wires from Kaiser Marquardt Lot Nos. 1 and 2 screens, following the braze simulation heat treatment, was easily accomplished without any evidence of fusion between wires at the crossovers. SEM did not reveal any evidence of dislodged grains, dissolution of grain boundaries, voids at the grain boundaries, or fusion between wires for the heat treated Lot No. 1 or 2 wires.

14. The elements detected by SIMS analyses of cross sections of Pt-Ir wires on Meshes A and B were generally consistent with the bulk chemical analysis for this lot of wire. Exceptions were the detection of aluminum that was not detected by the bulk analysis and indium that was not checked for in the bulk analysis. Elemental mapping indicated that indium was uniformly distributed throughout the cross section.

15. SIMS analyses of cross sections of Kaiser Marquardt Lot No. 2 Pt-Ir screens showed reduced levels of impurities as compared to the S/N KM004 mid-screens, except for a strong manganese peak. No indium was detected for Lot No. 2.

16. SIMS analyses of wire surfaces for Mesh A identified different impurities adjacent to cracks as compared to undamaged areas. High levels of silicon and calcium were detected on the surfaces at all points, but quickly diminished during sputtering. The silicon and calcium my have originated from the diffusion pump oil contamination. As the silicon and calcium diminished during sputtering, significant levels of gallium, indium, manganese, and copper were detected adjacent to cracks. Substantially lower levels of these elements, particularly gallium and manganese, were detected at apparently undamaged areas.

17. SIMS analyses of wire surfaces for Mesh B were consistent with the apparently undamaged areas on Mesh A. Analysis of a saddle point on Mesh C was also consistent with the undamaged areas on Mesh A, except that somewhat higher levels of chromium, manganese, and indium were detected. The surface analysis of a high point at a crossover on

26

Mesh C was similar to the areas adjacent to cracks on Mesh A. Significant levels of gallium, indium, manganese, and copper were present. Indium and gallium increased during sputtering. Following SIMS analysis, a crack was detected by SEM at a high point on one Pt-Ir wire of the Mesh C sample.

The most common causes of brittle, intergranular failures in metals and alloys are hydrogen embrittlement, stress corrosion cracking, the formation of brittle phases at grain boundaries, the formation of low-melting-point phases at grain boundaries, and liquid-metal embrittlement. Platinum and its alloys are not generally susceptible to stress corrosion cracking or hydrogen embrittlement. Furthermore, these are delayed failure mechanisms that are characterized by slow crack propagation under sustained tensile stresses. The fact that wires extracted from Mesh A exhibited ductile tensile fractures at room temperature, but failed in a brittle, intergranular manner at 900°C (1650°F) are inconsistent with stress corrosion cracking or hydrogen embrittlement. This observation is, however, consistent with either the formation of low-melting-point phases at grain boundaries or liquid-metal embrittlement. These two mechanisms are the most likely candidates for causing the mid-screen fractures.

Liquid-metal embrittlement (LME) is the catastrophic brittle failure of a normally ductile metal when coated with a thin film of a liquid metal and subsequently stressed in tension.[8] The fracture is usually brittle intergranular, with little indication of crack branching or striations to indicate slow crack growth. In general, LME fracture surfaces are completely covered by the liquid metal. However, in some cases very small quantities of liquid are required, making detection of the liquid metal on the fracture surface very difficult. LME is usually caused by low-melting-point metals. Liquid metals that have been reported to cause LME include lead, bismuth, cadmium, mercury, lithium, zinc, gallium, indium, and many others. The fact that Ga and In were identified on the Pt-Ir wire surfaces adjacent to brittle cracks is a strong indicator that the fractures were caused by LME by one of these elements or by a Ga-In alloy. No reports of LME of Pt or its alloys by In or Ga were found in the literature. However, Ga and In have been reported to cause LME in several other face-centered cubic metals, including Al and Cu. LME usually occurs at temperatures near the solidification temperature of the liquid. An increase in temperature usually decreases embrittlement, leading to a brittle-to-ductile transition. In the present case, the experimental results for tensile tests on extracted wires suggested that the Pt-Ir wire was ductile at low temperatures (23 and 300°C; 73 and 570°F), but brittle at 900°C (1650°F). The melting points for Ga and In are 30 and 156°C (86 and 313°F), respectively. Thus, LME would be expected to occur at lower temperatures. On the other hand, Mn and Cu were associated with the Ga and In on the wire surfaces. Thus, a more complex LME interaction may have occurred.

Another potential embrittlement mechanism is the formation of low-melting eutectic or intermediate phases at the grain boundaries. In this case, the alloy usually fails in a ductile mode at temperatures up to or approaching the melting point of the grain boundary phase and in a brittle fashion at higher temperatures. The Pt-Ga and Pt-In phase diagrams[9, 10] (Figures 20 and 21) demonstrate that these systems form several intermediate phases with melting points below 900°C (1650°F). This embrittlement mechanism is quite common for Pt alloys and has been reported to occur due to contamination with low concentrations of Si, Ag, K, Pb, and Se.[1,7] Like the liquid in LME, the embrittling phase is usually easily detected on the brittle fracture surface, but in some instances is present in monolayers that are not easily detected.[7,11,12]
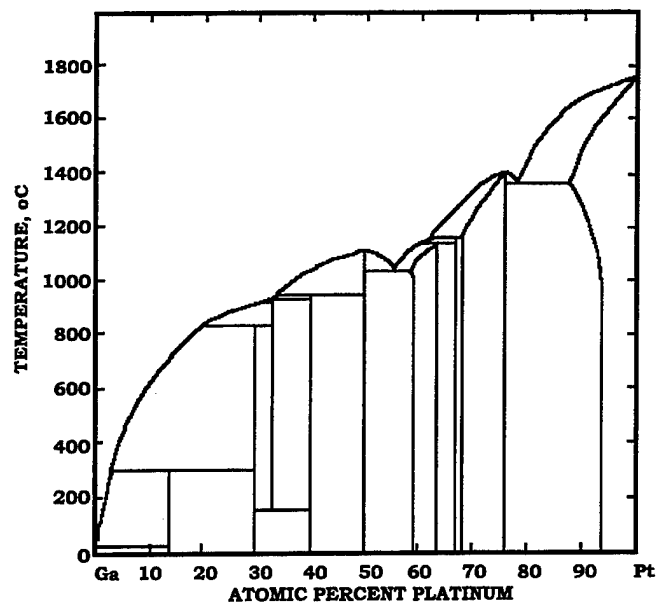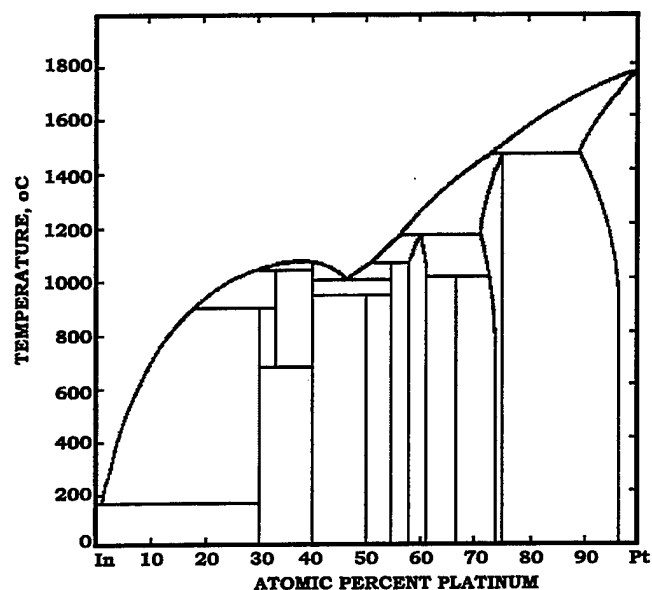
27

Figure 20. Platinum-gallium phase diagram.

Figure 21. Platinum-indium phase diagram.

Many aspects of the mid-screen failure on S/N KM004 are consistent with either liquid-metal embrittlement or the formation of a low melting phase at the grain boundaries. It is concluded that one of these mechanisms probably caused the failures. Ga and In are the most probable contaminants for causing the embrittlement. However, there may have been other factors that contributed to the failure. The partial fusion between wires at the crossover points of the weave along with the dissolution of grain boundaries, voids at grain boundaries, and dislodging of grains at the saddle points of the crossovers are indicators of abnormal behavior. The causes for this instability in the grain

28

boundaries at the saddle points were not determined. These observations may be consistent with contamination with Ga and/or In, but insignificant levels of Ga were detected at these locations, and the In concentrations did not appear to be any higher than in the bulk alloy. Furthermore, these abnormalities were observed at the saddle points of the Mesh B wires as well as the Mesh A wires. No brittle fractures or cracks were found on Mesh B. Furthermore, wires extracted from Mesh B exhibited ductile fracture features at all test temperatures when pulled to failure at 23, 850, and 950°C (73, 1560, and 1650°F). Nevertheless, the abnormalities present at the saddle points must be considered indicators of embrittlement and should be avoided.

A careful evaluation of the Lot Nos. 1 and 2 screens in Kaiser Marquardt's inventory revealed that these wires did not exhibit any of the abnormalities observed on the S/N KM004 mid-screen wires. Furthermore, even after two heat-treatment cycles simulating the brazing operation, no evidence of fusion between wires or abnormal grain boundary behavior was seen. The Kaiser Marquardt wire is manufactured by a different supplier, is woven into screen by a different weaver, and is fabricated into thrust chamber catalyst bed screens by a different manufacturer. Therefore, all Kaiser Marquardt REMs are exonerated of any concerns of Pt-Ir screen embrittlement.

The spacecraft contractor also has several REMs that were manufactured by Hamilton Standard. These REMS have been exonerated on the basis that they were manufactured at a time different from the mid-retainer/screen assembly on S/N KM004, and that they utilized Pt-Ir wire from different lots. The end retainer/screen assembly from S/N KM004 also had a lot of wire different from the mid-retainer/screen assembly. No evidence of embrittlement was observed on the end screens. It is recommended that additional inspections of the end screens be performed. The nozzle end retainer/screen assembly is being maintained as a spare and not to be disassembled. However, it should be possible to inspect the wires for evidence of fusion at the crossover points on the weave. If no evidence of fusion is observed, this will help to exonerate the other Hamilton Standard REMs. If evidence of fusion is found, additional inspection of the end retainer/screen assembly should be considered.

References

1. B. McLemore, "Mark II - Brittle Pt-Ir Catalyst Screen Wire Failure on P/N SV779040-3, S/N KM004," Kaiser Marquardt Process Memorandum No. 14.448, April 15, 1998.

2. A. G. Knapton, "Ensuring the Most Advantageous Use of Platinum," *Platinum Metal Review*, Vol. 23, No. 1, pp. 2–13, 1979.

3. V. V. Stepanov and V. A. Dmitriev, "Causes of Local Embrittlement of Platinum Alloys in Argon-Arc Welding," *Welding Production*, Vol 24, No. 12, pp. 13–15, 1977.

4. F. E. Bemish, W. A. McBryde, and R. R. Barefoot, "The Platinum Metals," in *Rare Metals Handbook*.

5. "Platinum and Platinum Alloys," in *Metals Handbook, Vol. 2, 10th Edition, Properties and Selection: Nonferous Alloys and Special Purpose Materials*, ASM International, pp. 707–714, 1990.

6. M. R. Hilton, "Telecons with Oil Suppliers," Interoffice Correspondence No. 98-5651-MRH-2, The Aerospace Corporation, December 15, 1997.

7. C. L. White, J. R. Keiser, L. Heatherly, and J. F. Newsome, "Intergranular Embrittlement of Pt-30% W by Se Vapor," *Scripta Metallurgica*, Vol. 13, pp.543–547, 1979.

8. M. H. Kamdar, "Liquid-Metal Embrittlement," in *Metals Handbook Ninth Edition, Vol. 13, Corrosion*, ASM international, pp. 171–184, 1987.

9. W. G. Moffett, *The Handbook of Binary Phase Diagrams*, General Electric Company, Schenectady, N. Y., 1978.

10. *Journal of Less Common Metals*, Vol. 46, pp. 101–116, 1976.

11. C. L. White, J. R. Keiser, L. Heatherly, and J. F. Newsome, "The Effect of Se Partial Pressure on Intergranular Embrittlement of Pt-30% W Alloy," *Scripta Metallurgica*, Vol. 15, pp. 805–808, 1981.

12. J. M. Rosen and W. T. McFarlen, "Failure Mechanism Characterization of Platinum Alloy," in *International Instrumentation Symposium*, Instrumentation Society of America, pp. 625–630, 1986.

TECHNOLOGY OPERATIONS

The Aerospace Corporation functions as an "architect-engineer" for national security programs, specializing in advanced military space systems. The Corporation's Technology Operations supports the effective and timely development and operation of national security systems through scientific research and the application of advanced technology. Vital to the success of the Corporation is the technical staff's wide-ranging expertise and its ability to stay abreast of new technological developments and program support issues associated with rapidly evolving space systems. Contributing capabilities are provided by these individual Technology Centers:

Electronics Technology Center: Microelectronics, VLSI reliability, failure analysis, solid-state device physics, compound semiconductors, radiation effects, infrared and CCD detector devices, Micro-Electro-Mechanical Systems (MEMS), and data storage and display technologies; lasers and electro-optics, solid state laser design, micro-optics, optical communications, and fiber optic sensors; atomic frequency standards, applied laser spectroscopy, laser chemistry, atmospheric propagation and beam control, LIDAR/LADAR remote sensing; solar cell and array testing and evaluation, battery electrochemistry, battery testing and evaluation.

Mechanics and Materials Technology Center: Evaluation and characterization of new materials: metals, alloys, ceramics, polymers and composites; development and analysis of advanced materials processing and deposition techniques; nondestructive evaluation, component failure analysis and reliability; fracture mechanics and stress corrosion; analysis and evaluation of materials at cryogenic and elevated temperatures; launch vehicle fluid mechanics, heat transfer and flight dynamics; aerothermodynamics; chemical and electric propulsion; environmental chemistry; combustion processes; spacecraft structural mechanics, space environment effects on materials, hardening and vulnerability assessment; contamination, thermal and structural control; lubrication and surface phenomena; microengineering technology and microinstrument development.

Space and Environment Technology Center: Magnetospheric, auroral and cosmic ray physics, wave-particle interactions, magnetospheric plasma waves; atmospheric and ionospheric physics, density and composition of the upper atmosphere, remote sensing, hyperspectral imagery; solar physics, infrared astronomy, infrared signature analysis; effects of solar activity, magnetic storms and nuclear explosions on the earth's atmosphere, ionosphere and magnetosphere; effects of electromagnetic and particulate radiations on space systems; component testing, space instrumentation; environmental monitoring, trace detection; atmospheric chemical reactions, atmospheric optics, light scattering, state-specific chemical reactions and radiative signatures of missile plumes, and sensor out-of-field-of-view rejection.